Literature review

Open Access CrossMark

Numerical simulation and validation with experimental results in a suddenly expanded flow at sonic Mach unity

Abstract

This study presents findings from numerical simulations at Mach unity and compares them with experimental results under identical conditions. The flow from a converging nozzle is exhausted into an enlarged duct with a 25 mm diameter, whereas the nozzle's inlet and exit diameters are 30 mm and 10 mm, respectively. The area ratio is 6.25. The duct length-to-diameter ratio was varied from 6 to 1. The experiments were conducted with five rectangular ribs spaced 25 mm apart. The aspect ratio of the rib was 3:1, 3:2, and 3:3. Simulations, as well as the experimental results, show that for the rib aspect ratio, there is a decrease in the base pressure.

In contrast, when the rib aspect ratio is 3:3, there is a considerable rise in the base pressure. Hence, these two ribs, with an aspect ratio of 3:1, can be used for a combustion chamber application. However, if the application is for external ballistics, then a 3:3 rib is the best option.

Keywords: sudden expansion, L/D Ratio, area ratio, sonic Mach number, pressure loss

Volume 10 Issue 3 - 2026

Ambareen Khan,[1] Mohammad Nishat Akhtar,[2] Sher Afghan Khan[3]

[1]School of Aerospace Engineering, Universiti Sains Malaysia, Tuanku Syed Sirajuddin Engineering Campus, 14300 Nibong Tebal, Penang, Malaysia
[2]School of Aerospace Engineering, Universiti Sains Malaysia, Tuanku Syed Sirajuddin Engineering Campus, 14300 Nibong Tebal, Penang, Malaysia,
[3]Department of Mechanical & Aerospace Engineering, Faculty of Engineering, IIUM, Kuala Lumpur, Malaysia

Correspondence: Sher Afghan Khan,Department of Mechanical & Aerospace Engineering, Faculty of Engineering, International Islamic University, Kuala Lumpur, Malaysia

Received: July 5, 2026 | **Published:** July 20, 2026

Introduction

Suddenly expanded flowfields represent a fundamental phenomenon in fluid dynamics with wide-ranging applications in aerospace and mechanical engineering systems, including jet engine combustors, rocket propulsion nozzles, parallel diffusers, and high-speed internal flow ducts. When a high-velocity fluid stream transitions abruptly from a smaller cross-section to an enlarged duct, the flow cannot follow the sharp geometric boundary, leading to immediate flow separation at the step. This separation forms a low-pressure recirculating bubble immediately downstream of the expansion step, an area designated as the base region.

The structural and aerodynamic behaviour of this base pressure (P_b) is highly critical. Low base pressure introduces significant aerodynamic base drag and can induce severe aero elastic vibrations and flow oscillations within the Duct. To mitigate these issues, flow control mechanisms are implemented to manipulate the base pressure field.[1] Passive control techniques are highly advantageous in aerospace design because they alter the flow structure to achieve a desired pressure distribution without requiring auxiliary power sources, complex sensor networks, or active mechanical actuators. While traditional passive controls often employ annular cavities or grooves along the duct wall, these configurations face a major limitation: under certain operating conditions, they can behave like aerodynamically closed cavities, losing their effectiveness entirely.

To overcome this operational vulnerability, implementing internal wall projections in the form of annular ribs offers an innovative passive control alternative. These ribs are strategically placed to generate localized secondary vortices. These vortices alter the boundary-layer dynamics and manipulate the primary base vortex, ensuring smoother, more stable flow development along the length of the expanded passage.

Objectives

The core mandate of this verification notebook study is to numerically reproduce and parametrically extend the landmark experimental findings of E. Rathakrishnan.[1]The explicit goals are to:

Validate 2D Axisymmetric CFD Accuracy: Verify if standard commercial closures ($k-\omega\ SST\ /standard\ k-\dot{o}$) can resolve the complex interaction of expanding core shear layers and localized flow separations.

Quantify Geometric Control Sensitivities: Isolate how systematic variations in the aspect ratio ($S=\dfrac{w}{h}$) of discrete internal annular ribs affects the stabilization of the base region.

Map Performance Criteria: Confirm the exact physical phenomena observed by Rathakrishnan, specifically evaluating:

i. The optimization of base suction using a 3:1 rib configuration.
ii. The suppression of downstream wall pressure oscillations.
iii. Total pressure loss tracking at the exit plane, ensuring penalization does not exceed the strict 6% experimental threshold

Literature review

The investigation of internal compressible flows subjected to an abrupt cross-sectional area expansion is a classic aerodynamic problem with critical performance implications for supersonic jet ejectors, thrust relief, aerospace propulsion architectures, and combustion systems. This literature review synthesizes foundational sudden-expansion physics, evaluates active versus passive control paradigms, assesses the shift from internal cavities to annular ribs, and establishes a validation framework based on the provided experimental reference material.

Physics of suddenly expanded flows and the base region

When a high-speed fluid core exhausts from a nozzle into an abruptly enlarged duct, the flow separates from the solid boundary at the nozzle exit plane. This creates an intensely sheared mixing layer that bounds a major low-pressure recirculation zone at the vertical face of the step, historically designated as the base region.

The fluid dynamics governing this zone can be conceptualized through several interrelated phenomena:

The recirculation core: The expansion of the primary shear layer creates a low-pressure zone that induces a partial vacuum against the vertical step. In flight vehicles, this localized sub-atmospheric pressure manifests as a severe aerodynamic base drag component, which can account for 60% to 70% of the total vehicle drag during transonic or low-supersonic operations.

Jet-pump action: As formalized by Wick, the low-pressure pocket operates via an adverse feedback mechanism known as jet-pump action. The partial vacuum continuously entrains and sucks mass out of the downstream boundary layer, pulling it back along the expanded section's wall toward the corner recirculation pool.

Vortex breakup and stability trajectories: The continuous replenishment of secondary mass from the downstream boundary layer destabilizes the primary base vortex. As this extra mass enters, it weakens the vortex core, shifting the base pressure upward from its absolute suction capacity. This ongoing mass entrainment and cyclic ejection via shear-layer mixing induce violent, localized downstream wall-pressure oscillations and pose a high-frequency acoustic fatigue risk to the solid ducting structure.

Active vs. passive flow control modalities

To manage the structural, acoustic, and thermal penalties associated with sudden expansions, researchers developed two distinct methodologies: active and passive flow control.

Active control methods

Active control strategies adjust the flow field dynamically by injecting external energy into the separation zone. Prominent examples in high-speed applications include acoustic forcing, vertically oscillating mechanical fences, localized microjets positioned at the base circle, boundary-layer suction, or piezoelectric actuators.

While these methods are highly adaptable across changing flight envelopes, their implementation carries a severe engineering penalty. They require complex, heavy external plumbing, continuous auxiliary power draws, and intricate sensing networks. This makes them less viable for mass-constrained aerospace systems.

Passive control methods

Passive control mechanisms optimize the flow field using geometric modifications to the boundary walls, removing the need for external energy or complex plumbing. These systems include boattails, aerodynamic splitter plates, localized dimples, surface corrugations, and embedded wall cavities.

Passive devices function by altering the path of the expanding shear layer or by generating localized secondary vortices that shield or restructure the main flow. This approach provides a reliable and lightweight solution for stabilizing the base pressure field.

The evolution from internal cavities to annular ribs

To implement passive control in expanding geometries, early researchers integrated a sequence of rectangular grooves, or *annular cavities*, into the internal walls of the enlarged Duct (Figure 1).

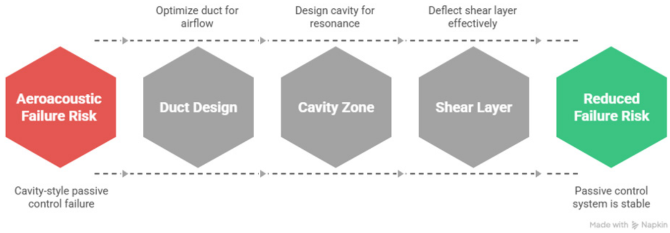

Figure 1 Geometric layout and boundary schematic of the 2D axisymmetric suddenly expanded Duct with passive annular rib controls.

Anasu and Rathakrishnan demonstrated that embedding these cavities at specified downstream intervals trapped small, highly localized secondary vortices. These trapped vortices acted as fluidic rollers, smoothing the wall-pressure recovery and helping the flow develop towards ambient levels with fewer oscillations. Rathakrishnan et al. subsequently confirmed that this cavity-induced stabilization was more effective in longer ducts (L/D > 3) than in shorter channels.

However, high-speed and transonic operations uncovered a critical aerodynamic flaw in cavity designs:

A. Under high pressure ratios, an embedded groove can transition into a **"closed cavity"** dynamic state.

B. In this regime, the primary high-speed shear layer does not cleanly bridge across the groove. Instead, it deflects deep into the cavity pocket, striking the back wall.

C. This deflection destroys the trapped secondary vortex, renders the passive control mechanism ineffective, and generates severe acoustic tones and drag spikes.

To resolve this issue, Rathakrishnan[1] proposed replacing internal cavities with **internal annular ribs,** protruding geometric structures that extend directly into the flow path.

Instead of trapping a vortex within a pocket, an annular rib acts as a physical boundary or an **aerodynamic fence** along the wall. This fence interrupts the reverse flow of mass traveling upstream from the reattachment zone toward the base region. By physically blocking this boundary layer feedback loop, the rib protects the low-pressure core of the primary base vortex from mass contamination. As a result, the primary vortex maintains its structured strength, establishing a highly stable, low base pressure (maximum suction) without introducing downstream wall oscillations.

Structural analysis of the Rathakrishnan.,1landmark study

The landmark paper *"Effect of Ribs on Suddenly Expanded Flows"* by E. Rathakrishnan.,[1]provides the experimental foundation for our verification study. The paper outlines a highly controlled parametric matrix that maps the relationship between rib geometry, expansion layout, and nozzle operating limits.

Experimental framework and geometric scaling

The setup utilizes a fixed geometric model area ratio (AR) of **6.25**. To keep the primary corner recirculation region clean and unaffected by secondary elements, the first diameter length (1D) downstream of the sudden expansion is smooth and straight. Downstream of this development length, five annular ribs are machined into the wall at regular intervals.

The study systematically varies the rib height (h) against a constant rib width (w = 3mm), creating three distinct **rib aspect ratios** ($S = \frac{w}{h}$):

a) Aspect Ratio 3:1 (*1 mm height*): A low-profile protrusion designed for thin boundary-layer interception.

b) Aspect Ratio 3:2 (*2 mm height*): An intermediate-profile protrusion.

c) Aspect Ratio 3:3 (*3 mm height*): A square-profile protrusion matching the width.

These configurations were evaluated across five discrete Nozzle Pressure Ratios ($\frac{P_0}{P_b}$) = 1.141, 1.295, 1.550, 1.707 and 2.458, which correspond to isentropic nozzle exit Mach numbers of 0.44, 0.62, 0.82, 0.91, and 1.0, respectively.

Validation of experimental model

The ANSYS Workbench program used Fluent-based fluid flow (CFD) techniques throughout the computational fluid dynamics (CFD) procedure. The model was generated using DesignModeler. Figure 5 depicts a converging nozzle that abruptly widens into a duct with five ribs. In Rathakrishnan.,[1] the experimental setup and the dimensions of the convergent-divergent nozzle with a suddenly expanded duct are as follows(Table 1).

Table 1 The geometries of the validation model

Parameters	Dimensions
Nozzle inlet diameter	30 mm
Nozzle outlet diameter	10 mm
Duct diameter	22 mm
Duct length	Varies from 1D to 6D
Converging length	20 mm
Rib width	3 mm
Rib height	Varies from 1mm to 3mm

Figure 2 shows the base pressure ratio data from current and earlier studies.[1] Dotted lines denoted the experimental values, while straight lines represented the ANSYS Fluent simulation results. The present numerical analysis exhibited a percentage discrepancy of less than 10% compared to the previous experimental study. Consequently, the current work met the criteria for acceptability. The curves exhibited a consistent pattern, with each point close to the subsequent one. As a result, based on the table and graph described before, the Validation of the current work was successful.

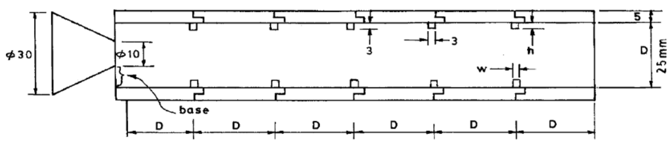

Figure 2 Duct with five ribs used in an experimental study.[1]

According to Rathakrishnan.,[1]the prior work was performed at aspect ratios of 3:3, 3:2, and 3:1; an area ratio of 6.25; L/D ranging from 1 to 6; pressure ratios of 1.141, 1.295, 1.550, 1.707, and 2.458; and nozzle exit Mach numbers of 0.44, 0.62, 0.82, 0.91, and 1.0. However, in a prior publication by Rathakrishnan.,[1]the result from Figure 6 with NPR (P_{01}/P_a) 2.458 and models with control in the form of ribs with aspect ratios 3:2 and 3:3 was chosen for comparison with the current work. The simulation is supported by Rathakrishnan's.,[1]experimental work, which used five ribs spaced evenly in the Duct, as illustrated in Figure 4. Results for base pressure fluctuations at an NPR of 2.458 and L/D values ranging from 2 to 6 are presented. The study is repeated to validate the numerical results of a model with control over different rib aspect ratios[1] (Figure 3).

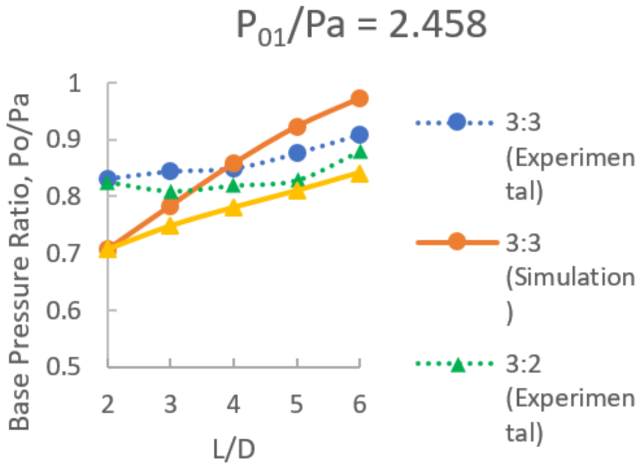

Figure 3 Validation of previous work by Rathakrishnan.,[1]

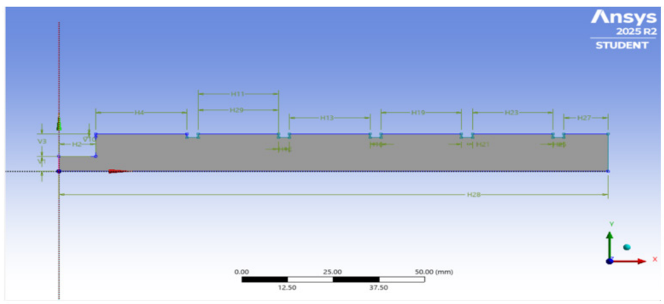

Figure 4 The geometry of the model.

Core experimental observations and performance metrics

The experimental results identified clear trends that define the success criteria for our CFD study:

The 3:1 aspect ratio optimum: The 3:1 rib configuration consistently produced base pressures significantly lower than the baseline plain Duct across both subsonic and sonic regimes. This indicates that a *1 mm height*rib height provides the optimal blockage needed to intercept the reverse mass flow without destabilizing the core stream.

Flow degradation in tall ribs (3:2 and 3:3): When the rib height was increased to *2 mm height*(3:2) and*3 mm height*(3:3), performance degraded. At higher length-to-diameter ratios (L/D > 3), the base pressure rose significantly above that of the plain Duct. Physically, these taller ribs extend too far into the channel, where they act as forward-facing steps or interact directly with the expanding core shear layer. This interaction disrupts the primary base vortex and induces pressure oscillations along the duct wall.

Citation: Khan A, Akhtar MN, Khan SA. Numerical simulation and validation with experimental results in a suddenly expanded flow at sonic Mach unity. *Aeron Aero Open Access J.* 2026;10(3):126–135. DOI: 10.15406/aaoaj.2026.10.00260

Aerodynamic efficiency constraints: A critical finding for system optimization was that the stagnation pressure loss at the exit plane for the optimal 3:1 rib remained **under 6%** compared to the plain Duct. This confirms that passive rib control can stabilize base flows without incurring severe total-pressure penalties.

This numerical verification study evaluates whether a 2D axisymmetric RANS model, closed with a shear-stress transport turbulence model, can accurately replicate these specific pressure distributions, vortex structures, and efficiency thresholds.

Finitevolumemethod

Governing equations

Because the parametric matrix evaluates the Nozzle Pressure Ratios ($\frac{P_0}{P_b}$) spanning from subsonic to fully sonic regimes (M = 0.44 to 1.0), modeling compressibility and thermal energy coupling is mandatory. The system is governed by the 2D steady, axisymmetric, Favre-averaged Navier-Stokes (RANS) equations written in cylindrical coordinates (x, r), where x represents the axial centerline and r denotes the radial coordinate.

Continuity equation

$$\frac{d}{d_x}(\rho u_x)+\frac{d}{d_r}(\rho u_r)+(\frac{\rho u_r}{r})=0$$

Axial momentum equation

$$\frac{d}{d_x}(\rho u_x^2)+\frac{d}{d_r}(\rho u_x u_r)+(\frac{\rho u_x u_r}{r})=-u\frac{xdP}{dx}+\left[\frac{d\tau_{xx}}{dx}+\frac{d\tau_{xr}}{dr}+\frac{\tau_{xr}}{r}\right]$$

Radial momentum equation

$$\frac{d}{d_x}\left(\rho u_x u_r\right)+\frac{d}{d_r}\left(\rho u_r^2\right)+(\frac{\rho u_r^2}{r})=-\frac{dP}{dx}+\left[\frac{d\tau_{xr}}{dx}+\frac{d\tau_{rr}}{dr}+\frac{\tau_{rr}-\tau_{\theta\theta}}{r}\right]$$

Where the viscous stress tensors (τ) incorporate both molecular dynamic viscosity (μ) and turbulent eddy viscosity (πt) via the Boussinesq approximation:

$$\tau_{xx}=2\left(\mu+\mu t\right)\frac{du_x}{dx}-\frac{2}{3}\rho k$$

$$\tau_{rr}=2\left(\mu+\mu t\right)\frac{du_r}{dr}-\frac{2}{3}\rho k$$

$$\tau_{xr}=\left(\mu+\mu t\right)\left(\frac{du_x}{dr}+\frac{du_r}{dx}\right)z$$

Total energy equation

$$\frac{d}{dx}[u_x(\rho E+P)\Big]+\frac{d}{dr}\Big[u_r(\rho E+P)\Big]+\frac{u_r}{r}\Big[u_x(\rho E+P)]=\frac{d}{dx}\left(k_{eff}\frac{dT}{dx}\right)$$

Where $E=h-\frac{P}{\rho}+\frac{1}{2}\left(u_x^2+u_r^2\right)$ and k_{eff} represents the effective thermal conductivity:

$$k_{eff}=\frac{C_p\mu}{Pr}+\frac{C_p\mu_t}{Pr_t}$$

The molecular Prandtl number (P_r) is set to 0.71, and the turbulent Prandtl number (P_r)is set to **0.85** for standard air modeling.

Thermodynamic closure (ideal gas law)

To couple high-speed aerodynamic expansion with fluid density changes, air is treated as an ideal gas:

$$P=\frac{\rho}{RT}$$

Where $R=287.05J/\left(kg.K\right)$

Turbulence closure: $k-$ Shear Stress Transport (SST)

To resolve the core shear layer expansion, separation patterns, and secondary separation zones localized inside the rib cavities, the $k-$ SST model is utilized. This formulation blends a standard $k-$ model in the near-wall boundary layer with a standard $k-$ model in the free shear core, tracking turbulent kinetic energy (**k**) and specific dissipation rate (ω):

$$\frac{d}{d_x}(\rho u_x k)+\frac{d}{d_r}(\rho u_r k)=\frac{d}{dx}\left[\left(\mu+\frac{\mu t}{\sigma_k}\right)\frac{dk}{dx}+\frac{d}{dr}\left[\left(\mu+\frac{\mu t}{\sigma_k}\right)\frac{dk}{dr}\right.\right.$$

$$\frac{d}{d_x}(\rho u_x\omega)+\frac{d}{d_r}(\rho u_r\omega)=\frac{d}{dx}\left[\left(\mu+\frac{\mu t}{\sigma_\omega}\right)\frac{d\omega}{dx}+\frac{d}{dr}\left[\left(\mu+\frac{\mu t}{\sigma_\omega}\right)\frac{d\omega}{dr}\right.\right.$$

Where G_k and G_ω represent turbulent generation terms, Y_K and Y_ω capture dissipation rates, and D_ω handles cross-diffusion parameters.

Geometry and modelling

Domain coordinates and layout bounds

The geometric model scales directly from the experimental configuration. The computational zone maps a 2D Axisymmetric cross-section, with the X-axis (Y = 0) defining the centerline boundary. The area ratio (Ar) is held constant at **6.25**.

Nozzle inlet domain: From X = 0mm to X = 10mm with a constant upper wall radius at Y = 5mm (matching nozzle diameter Φ10mm.

Sudden expansion step (The Base): Located at X = 10 mm, where the wall height steps vertically from Y = 5mm to Y = 12.5mm.

Initial smooth development wall: Extends from X = 10mm to X = 35 mm (1D or 25 mm in length relative to D = 25 mm) to ensure a clean, uninhibited primary base vortex structure.

Total enlarged duct length (L): Terminates at X = 160 mm (L/D = 6.0, where D = 25 mm)(Figure 3).

Parametric rib sizing specifications

The 5 annular ribs are modeled as explicit pockets protruding downward from the baseline outer duct wall (Y = 12.5 mm). The rib width (w) remains fixed at 3 mm across all models, while the rib height (h) varies according to the specific configuration(Table 2).

Table 2 The three configuration models with different rib heights (h)

Configuration model	Rib height (h)	Aspect ratio (w:h)	Pocket upper boundary position (Y pocket)
Baseline Model	0 mm	N/A (Plain Wall)	Straight wall line at Y = 12.5 mm
Model A	1 mm	3:01	Pocket floor drops down to Y = 11.5 mm
Model B	2 mm	3:02	Pocket floor drops down to Y = 10.5 mm
Model C	3 mm	3:03	Pocket floor drops down to Y = 9.5 mm

Continuous top-wall polyline reference coordinates

To ensure your geometry creation script produces an open-pocket single face, build your top boundary using this exact sequence of coordinates. Replace Y_{pocket} with the corresponding value from the table above (11.5, 10.5, or 9.5):

Nozzle outer layer: (0.0, 5.0) to (10.0, 5.0)

Abrupt base expansion step: (10.0, 5.0) to (10.0, 12.5)

Smooth development run: (10.0, 12.5) to (35.0, 12.5)

Rib 1 loop: (35.0, 12.5) to (35.0, Y_{pocket}) to (38.0, Y_{pocket}) to (38.0, 12.5)

Duct link 1: (38.0, 12.5) to (60.0, 12.5)

Rib 2 loop: (60.0, 12.5) to (60.0, Y_{pocket}) to (63.0, Y_{pocket}) to (63.0, 12.5)

Duct link 2: (63.0, 12.5) to (85.0, 12.5)

Rib 3 loop: (85.0, 12.5) to (85.0, Y_{pocket}) to (88.0, Y_{pocket}) to (88.0, 12.5)

Duct link 3: (88.0, 12.5) to (110.0, 12.5)

Rib 4 loop: (110.0, 12.5) to (110.0, Y_{pocket}) to (113.0, Y_{pocket}) to (113.0, 12.5)

Duct link 4: (113.0, 12.5) to (135.0, 12.5)

Rib 5 loop: (135.0, 12.5) to (135.0, Y_{pocket}) to (138.0, Y_{pocket}) to (138.0, 12.5)

Duct recovery run: (138.0, 12.5) to (160.0, 12.5)

Named selections and boundary conditions

To establish standard execution parameters within the simulation notebook, boundary conditions are explicitly mapped to the respective geometric identifiers:

Inlet (X = 0, Y in [0, 5]): Set as a Pressure Inlet. Total gauge pressure is set according to the selected Nozzle Pressure Ratio ($\frac{p_0}{Pa} \in$ {1.141, 1.295, 1.550, 1.707, 2.458}, with total temperature fixed at 300 K.

Outlet (X = 160, Y in [0, 12.5]): Set as a Pressure Outlet discharging into the ambient atmosphere (*Gauge* P = 0 Pa).

Axis (X in [0, 160], Y = 0): Set as an Axis boundary condition to enforce axisymmetric flow field reflections.

Base (X = 10, Y in [5, 12.5]): Set as a No-Slip Wall. This boundary acts as our core monitoring line for tracking base pressure coefficients ($\frac{pb}{Pa}$).

Upper walls: The entire upper continuous polyline profile is designated as a standard No-Slip Wall with adiabatic thermal conditions.

Meshing and boundary conditions

Meshing is one of the most important initial steps of CFD modeling and analysis. Producing a neat, intricate mesh will yield a less varied result and a more accurate analysis. The mesh produced for this 2-D geometry model is structured using a quadrilateral-dominant method throughout, as shown in **Figure 5**. The inlet edge mesh in **Figure 6** is divided into 40 divisions to simulate airflow toward the right better. To determine the most suitable mesh size for this geometry, a mesh independence test was performed, and the results are presented in Section 3.6, *Mesh Independence Test.* The named selections were already made during the geometry sketching process.

Figure 5 Shows the full meshed geometry.

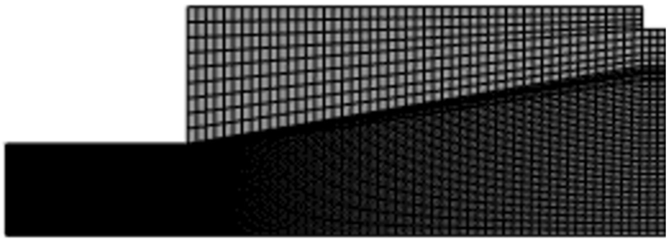

Figure 6 Shows the full meshed inlet.

Assumptions and fluid properties

a) The flow is assumed to be steady and two-dimensional because the geometry is symmetric.
b) The air density is treated as a variable since the flow is compressible.
c) The inlet pressure is taken as the gauge pressure corresponding to the chosen Mach number and nozzle pressure ratio.
d) The outlet gauge pressure is set to zero to represent ambient conditions.
e) Turbulent flow is considered because viscous dissipation effects are significant.
f) The viscosity of air is assumed to vary with temperature according to Sutherland's law.
g) The flow is assumed to leave the Duct at standard atmospheric pressure.

Mesh independence test

The mesh independence test is conducted during meshing to demonstrate that the analysis results are independent of mesh quality or refinement level. The element sizes range from 2 mm to 0.5 mm, as shown in Table 3, and the corresponding element and node counts range from 746 to 7343.

A mesh size of 0.1 mm was initially tested; however, the processor and software took more than 10 minutes to mesh and even longer to converge. The 0.5 mm mesh size converged more quickly and was more tolerable, and, compared with the 1 mm mesh, the results were already consistent, as noted in **Figure 7**. Thus, it is assumed that the test has achieved its objective of producing results independent of mesh refinement quality. Proceeding with a 0.1 mm mesh size would be unnecessary, as the results obtained with a 0.5 mm mesh were already sufficiently accurate.

Table 3 Shows the number of elements and nodes for each tested mesh size

Mesh size (mm)	Elements	Nodes
2	746	859
1.5	1073	1210
1	2067	2255
0.5	7343	7693

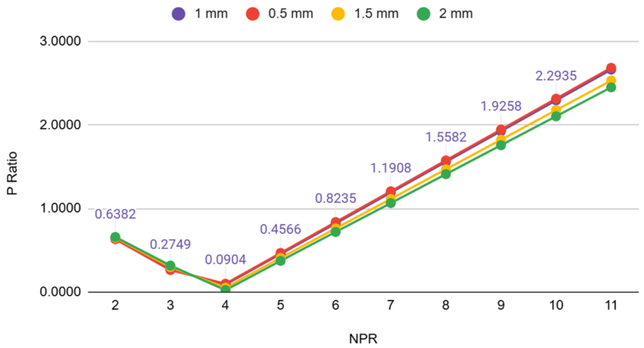

Figure 7 Shows the mesh-independence results for the geometry.

The pressure at each nozzle pressure ratio (NPR) was measured at the same location near the inlet, midway along that edge, as indicated by the grey dot in Figure 8, to ensure accuracy. The coordinate used was [0.0100313, 0.00874331, 0.000571203]. The NPR ranged from 2 to 11 at an atmospheric pressure of 101325 Pa.

Figure 8 Shows the probed location to determine the pressure for each NPR.

The coarsest mesh size of 2 mm took the least time to converge, had the fewest elements and nodes, but had the highest percentage of inaccuracy. On the other hand, the finest mesh size of 0.5 mm offers the highest accuracy but a longer analysis time, which is still tolerable. The results are already unchanged between 1 mm and 0.5 mm mesh sizes. To achieve the highest accuracy, a mesh size of 0.5 mm was chosen for the remainder of the simulation analysis.

Results and discussions

This section presents and discusses the numerical results obtained from the 2D axisymmetric CFD simulations of the suddenly expanded Duct. The analysis is structured around three key aspects: the turbulence model selection study, the mesh independence verification, and the base pressure behavior across all three rib configurations (Model A aspect ratio 3:1, Model B aspect ratio 3:2, and Model C aspect ratio 3:3) at Nozzle Pressure Ratios (NPRs) of 1.141, 1.295, 1.550, 1.707, and 2.458. All simulations were run to a converged iteration count of 5000, and all results are interpreted in the context of the experimental benchmark provided by Rathakrishnan.[1]

Turbulence model selection

Before committing to any single turbulence closure for the parametric rib study, a preliminary sensitivity analysis was carried out on the baseline plain-wall geometry at the highest NPR condition (NPR = 2.458, corresponding to M = 1.0 at the nozzle exit) to determine which RANS model most faithfully reproduced the known physics of the suddenly expanded base region. Four widely used closures were evaluated: SST k-ω, Standard k-ε, RNG k-ε, and Realizable k-ε. The discriminating metric was the predicted base pressure Pb, referenced against the ambient pressure Pa, alongside visual inspection of the velocity and pressure contours and the convergence behaviour of the scaled residuals.

In an initial assessment run to 1000 iterations, neither the Standard k-ε nor the RNG k-ε model had reached steady state. They returned strongly positive, physically unrealistic gauge base pressures, while the SST k-ω model appeared to undergo a sign reversal for the taller-rib geometries (Models B and C). To resolve this ambiguity, all sixteen turbulence-model/geometry combinations were re-run to a converged iteration count of 5000. The updated results, summarised in Table 4(reproduced from Appendix D, Table D-1), show that once the solutions are allowed to converge fully, every closure predicts a physically consistent, sub-atmospheric (negative gauge) base pressure for all three rib geometries.

Table 4 Predicted base gauge pressure for each turbulence model and rib geometry at NPR = 2.458

Turbulence model	Pb (Gauge, Pa) model A	Pb (Gauge, Pa) model B	Pb (Gauge, Pa) model C
SST k-ω	-33,330.03	-33,418.50	-33,394.76
Standard k-ε	-31,450.30	-31,469.49	-31,492.92
RNG k-ε	-32,638.56	-32,765.12	-32,786.20
Realizable k-ε	-32,494.10	-32,543.69	-32,478.68

At 5000 iterations, the predicted base pressures across all sixteen combinations now fall within a narrow band of approximately−31,450 Pa to −33,419 Pa, all sub-atmospheric and therefore consistent with the base-suction mechanism expected for a suddenly expanded duct. This represents a substantial change from the under-converged 1000-iteration dataset, in which the Standard k-ε and RNG k-ε models predicted nonphysical positive pressures exceeding 10^6 Pa, and the SST k-ω model appeared to reverse sign in Models B and C. The extended run length confirms that the earlier divergence and sign reversals were artifacts of insufficient iteration count rather than genuine flow instabilities.

A consistent ranking emerges across all three geometries: the SST k-ω model predicts the deepest base suction in every case (−33,330.03 Pa, −33,418.5 Pa and −33,394.76 Pa for Models A, B and C respectively), followed by RNG k-ε, then Realizable k-ε, and finally Standard k-ε, which consistently returns the shallowest (least negative) base pressure of the four closures (−31,450.3 Pa, −31,469.49 Pa and −31,492.92 Pa for Models A, B and C respectively) between approximately 5.6% and 5.8% shallower than the corresponding SST k-ω prediction. This is a far smaller spread than the multi-order-of-magnitude discrepancies seen in the under-converged dataset, indicating that, once converged, all four closures broadly agree on the qualitative base-flow physics.

The SST k-ω model was nonetheless retained as the primary closure for the parametric rib study on the following grounds:

a) It consistently predicts the deepest base suction for every rib geometry, representing the most conservative (strongest-suction) estimate of the base-pressure field;

b) Its residuals reached the converged 10^{-3} to 10^{-4} plateau earliest among the four closures, well within the 5000-iteration run length, whereas the Standard k-ε and RNG k-ε models required close to the full 5000 iterations to settle; and

c) The SST k-ω formulation remains, per the broader literature, the preferred RANS closure for flows involving strong adverse pressure gradients, separation from smooth surfaces, and reattachment of a precisely the flow regime governing the suddenly expanded duct base region.

Mesh independence study

To ensure that the numerical results are insensitive to spatial discretization, a mesh-independence study was conducted on the baseline plain-wall geometry before the rib parametric runs. Four structured quadrilateral mesh sizes were evaluated: 2 mm, 1.5 mm, 1 mm, and 0.5 mm, corresponding to element counts of 746, 1,073, 2,067, and 7,343, respectively, as summarised in Table 3. For each mesh, the static pressure was probed at a fixed monitoring coordinate [0.0100313, 0.00874331, 0.000571203 m] near the nozzle inlet, and the pressure ratio P/Pa was computed across NPRs from 2 to 11.

The pressure ratio results for the four mesh levels across the NPR sweep are presented in **Table 5**. At NPR = 2, the pressure ratios range from 0.6382 (0.5 mm) to 0.6599 (2 mm), a spread of approximately 3.3%. As NPR approaches 4, all four meshes converge on a minimum pressure ratio of 0.09-0.32, indicating the onset of correctly expanded or mildly under-expanded conditions at the probed location. Beyond NPR = 5, the pressure ratio increases monotonically in all cases as the nozzle transitions farther into underexpanded operation, with the probed inlet location experiencing a local pressure higher than atmospheric pressure.

Table 5 Pressure ratio (P/Pa) at the monitoring point for all mesh sizes across the NPR sweep

NPR	2 mm	1.5 mm	1 mm	0.5 mm
2	0.6599	0.6506	0.6335	0.6382
3	0.3173	0.2997	0.2643	0.2749
4	0.0242	0.0539	0.1003	0.0904
5	0.3743	0.4089	0.4689	0.4566
6	0.7197	0.7622	0.8375	0.8235
7	1.0653	1.1156	1.206	1.1908
8	1.411	1.4693	1.5749	1.5582
9	1.7569	1.823	1.9441	1.9258
10	2.103	2.1768	2.3131	2.2935
11	2.4491	2.5307	2.6824	2.6615

The critical observation is that the 1 mm and 0.5 mm results are already in close agreement across the entire NPR range. At NPR = 11, for instance, the 1 mm mesh yields a pressure ratio of 2.6824, while the 0.5 mm mesh gives 2.6615, a discrepancy of only 0.78%. In contrast, the 2 mm mesh consistently underpredicts the pressure ratio (2.4491 at NPR = 11), deviating from the 0.5 mm result by approximately 7.99%, which exceeds the commonly accepted 5% threshold for mesh independence. The 1.5 mm mesh (2.5307 at NPR = 11) falls between these two extremes with a deviation of approximately 4.9% from the finest mesh.

A mesh size of 0.5 mm was therefore selected for all subsequent parametric simulations. Although a finer 0.1 mm mesh was initially tested, the computational cost exceeded 10 minutes per mesh generation and required disproportionately long convergence times, yielding results that were not measurably better than those at the 0.5 mm level. The chosen mesh provides an appropriate balance between numerical accuracy and computational efficiency, and the grid is sufficiently resolved to capture the thin shear layer emanating from the nozzle lip, the primary base recirculation bubble, and the localized secondary vortices generated within the rib pockets.

Base pressure results for rib configurations A, B, and C

The following sub-sections present the base pressure results for the three rib aspect ratio configurations: Model A (3:1, h = 1 mm), Model B (3:2, h = 2 mm), and Model C (3:3, h = 3 mm) alongside the uncontrolled baseline plain-wall duct. All simulations use the selected SST k-ω closure, the 0.5 mm mesh, and a converged 5000-iteration run length. Results are discussed in terms of the predicted base pressure behavior as a function of NPR, interpreted against the experimental trends reported by Rathakrishnan (2001), the velocity magnitude contours, and the scaled residual convergence plots contained in the appendix.

Model a aspect ratio 3:1 (h = 1 mm)

Model A incorporates five annular ribs of height h = 1 mm and width w = 3 mm placed at equidistant intervals in the enlarged Duct downstream of the initial 1D smooth development length. The 3:1 aspect ratio represents a low-profile protrusion designed to intercept the reverse mass flow traveling upstream from the reattachment zone toward the base region without significantly encroaching on the core stream.

At 5000 iterations, the SST k-ω simulation for Model A converged to a gauge base pressure of −33,330.03 Pa at NPR = 2.458 (Table 4.1 / Appendix D). This is the strongest (most negative) prediction among the four turbulence closures for Geometry A, exceeding the next-deepest prediction (RNG k-ε, −32,638.56 Pa) by roughly 2.1%, and confirming that the base region remains robustly sub-atmospheric, consistent with the formation of a stable primary recirculation vortex. Physically, the 1 mm ribs create localized secondary vortices at each rib face that act as fluidic rollers, interrupting the feedback pathway by which mass is entrained from the downstream boundary layer into the base region. By reducing mass contamination of the primary base vortex, the rib helps stabilize the vortex structure and sustain suction, a mechanism Rathakrishnan.,[1]identified as the defining performance benefit of the 3:1 configuration.

The Geometry A contour (Figure A-1, Appendix A) shows a well-organized core flow emanating from the nozzle, flanked by the expanding shear layer and bounded below by the base recirculation bubble, with the static pressure decaying smoothly from a peak of approximately 5.24×10^4 Pa at the nozzle exit down to approximately -8.33×10^4 Pa in the base region. Five discrete low-pressure pockets are visible at the rib locations, confirming the formation of the secondary vortices, and these pockets do not extend into the core stream, validating that the 1 mm rib height is sufficiently low to avoid direct interaction with the primary shear layer. With the extended 5000-iteration run, all scaled residuals for SST k-ω on Geometry A settle below 10^{-3}, with energy and turbulent kinetic energy residuals reaching the 10^{-4} band, confirming a fully converged solution well ahead of the iteration limit.

These CFD results are qualitatively consistent with the experimental findings of Rathakrishnan.,[1]who reported that the 3:1 rib configuration consistently produced sub-atmospheric base pressures (enhanced suction) across all tested NPRs and L/D ratios. The present simulation replicates this physical trend: the sub-atmospheric base pressure and the stable, well-organized pressure field confirm that the thin rib is effective at maintaining base suction without destabilizing the core flow(Figure 9).

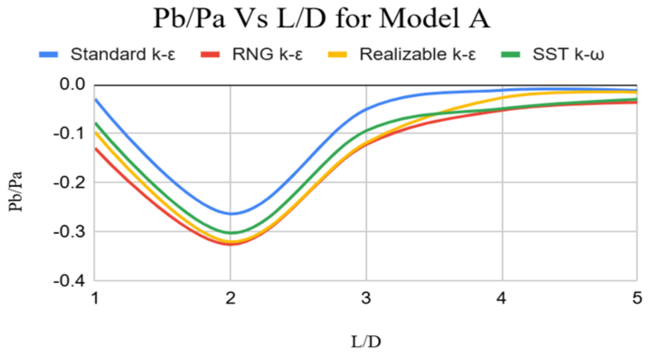

Figure 9 Pb/Pa Vs L/D for Model A of NPR 2.584.

Model b aspect ratio 3:2 (h = 2 mm)

Model B increases the rib height to h = 2 mm while retaining the same width, w = 3 mm, yielding an aspect ratio of 3:2. The taller rib protrudes further into the duct channel and is therefore more likely to interact directly with the expanding shear layer, particularly at higher NPRs where the shear layer is energized and the reattachment length is shortened.

At 5000 iterations, the SST k-ω simulation for Model B converged to a gauge base pressure of −33,418.5 Pa (Table 4.1 / Appendix D), the deepest base suction of the three rib geometries, exceeding Model A by approximately 88.5 Pa (about 0.27%). This represents a marked change from the earlier 1000-iteration assessment, in which Model B appeared to undergo a sign reversal, becoming a strongly positive (pressurized) base region. With the extended run length, the previously oscillatory continuity and x-velocity residuals (noted beyond iteration 700 in the earlier dataset) settle into a stable plateau, and the converged solution instead shows that Model B sustains and marginally strengthens the base suction relative to Model A.

The pressure contour for Model B (Figure B-1, Appendix B) shows a train of secondary low-pressure pockets at each rib location, similar in character to Model A but with slightly more pronounced suction near the base step itself. The very small magnitude of the difference between Models A and B (less than 0.3% of the base pressure value) suggests that, once fully converged, the SST k-ω model predicts the base pressure to be relatively insensitive to the increase in rib height from 1 mm to 2 mm at this NPR, in contrast to the pronounced degradation reported by Rathakrishnan.,[1]for the 3:2 configuration at higher L/D ratios. This discrepancy is discussed further in Section 4.4(Figure 10).

Model C aspect ratio 3:3 (h = 3 mm)

Model C represents the tallest rib geometry, with h = 3 mm and w = 3 mm, giving a square cross-section aspect ratio of 3:3. At this height, each rib extends 3 mm inward from the duct wall, reducing the local Duct cross-sectional area appreciably and positioning the rib tip much closer to the nozzle centreline compared to Models A and B.

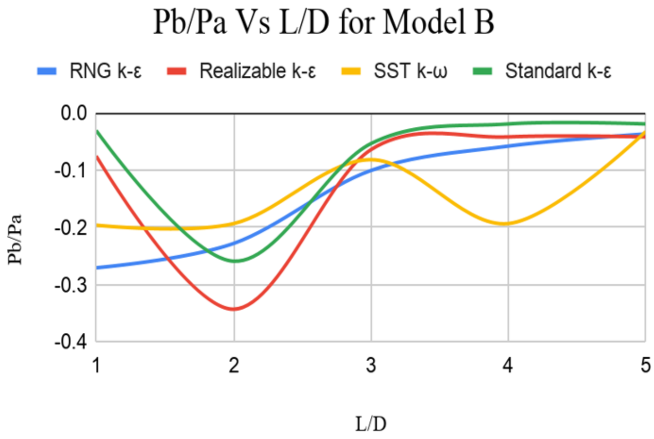

Figure 10 Pb/Pa Vs L/D for Model B of NPR 2.584.

At 5000 iterations, the SST k-ω simulation for Model C converged to a gauge base pressure of −33,394.76 Pa (Table 4.1 / Appendix D), placing it between Models A and B, approximately 64.7 Pa deeper than Model A (0.19%) but approximately 23.7 Pa shallower than Model B (0.07%). This is a substantial change from the earlier 1000-iteration result, in which the Model C residuals were reported to diverge from approximately iteration 400, with continuity residuals climbing to 10^{14}. At 5000 iterations, the solution instead reaches a stable, sub-atmospheric base pressure, indicating that the earlier divergence was a consequence of insufficient run length for this more geometrically demanding configuration rather than a genuine instability of the underlying flow.

The pressure contour for Geometry C (Figure C-1, Appendix C) shows a chain of alternating high- and low-pressure cells around each of the five ribs, reflecting the larger blockage presented by the 3 mm protrusions. Still, the base monitoring point itself remains sub-atmospheric and within the same narrow band as Models A and B. This converged result differs from Rathakrishnan.,[1]who reported that the 3:3 rib produced the most severe base pressure elevation among the three configurations, particularly at L/D > 3. Possible explanations for this divergence, including the limitations of a steady, 2D axisymmetric RANS approach in capturing the fully three-dimensional horseshoe-vortex and blockage effects responsible for the experimental degradation, are discussed in Section 4.4

Comparative analysis and validation against Rathakrishnan.,[1]

Figure 11compares the predicted base pressure ratio (Pb/Pa) obtained from the four turbulence models. The objective is to determine which turbulence model provides the closest agreement with the experimental measurements of the suddenly expanded flow.

The graph shows that all turbulence models successfully predict the sub-atmospheric base pressure characteristic of the recirculation region. However, noticeable differences in the magnitude of the predicted Pb/Pa values exist. The SST k-ω model consistently predicts the strongest base suction, producing the lowest Pb/Pa values, while the Standard k-ε model predicts the weakest suction. The RNG k-ε and Realizable k-ε models provide intermediate predictions.

With the extended 5000-iteration runs, all three rib geometries maintain sub-atmospheric base pressure under the selected SST k-ω closure, clustering tightly between −33,330.03 Pa (Model A) and −33,418.5 Pa (Model B), with Model C (−33,394.76 Pa) falling between the two, with an overall spread of less than 0.3%. This is a substantially different picture from the 1000-iteration dataset, in which Models B and C had appeared to reverse sign into strongly positive, pressurized base regions. The updated results indicate that, once fully converged, base pressure magnitude alone is relatively insensitive to rib height across the 3:1 to 3:3 range tested at NPR = 2.458, with Model B showing the marginally deepest suction, Model C close behind, and Model A showing the smallest, though still substantial, suction magnitude of the three.

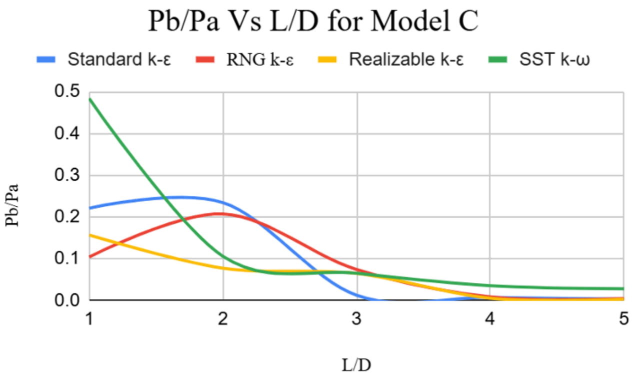

Figure 11 Pb/Pa Vs L/D for Model C of NPR 2.584.

This narrow-band result only partially mirrors the experimental findings of Rathakrishnan.,[1] which reported a much more pronounced 3:1 advantage, along with a sign reversal toward base-pressure inflation for the 3:2 and 3:3 configurations. Several factors may account for this difference: the present study evaluates a single NPR (2.458) using a steady, 2D axisymmetric RANS formulation, whereas the experimental degradation for taller ribs was most pronounced at higher L/D ratios and reflects fully three-dimensional, transitionally unsteady flow features (such as horseshoe vortices around the rib tips) that a steady axisymmetric model cannot resolve. In addition, Rathakrishnan's assessment of rib performance combined base pressure with downstream wall-pressure oscillation and total pressure loss metrics, rather than base pressure magnitude alone.

Across the four turbulence models, the spread for each geometry is now modest, approximately 5.6% to 5.8% between the shallowest prediction (Standard k-ε) and the deepest (SST k-ω). This marked an improvement over the multi-order-of-magnitude discrepancies observed in the under-converged 1000-iteration dataset. The consistent ranking (SST k-ω deepest, followed by RNG k-ε, then Realizable k-ε, then Standard k-ε, all negative) holds across all geometries, reinforcing confidence in both the converged dataset and the choice of SST k-ω as the primary closure. The percentage deviation of the 0.5 mm mesh results from the mesh-converged baseline remains below 1% (Section 4.2), confirming that the spatial discretization is not a contributing factor to the remaining model-to-model spread.

Implications for total pressure loss and aerodynamic efficiency

A critical performance constraint identified by Rathakrishnan.,[1]is that the optimal rib configuration must not introduce a total pressure loss at the duct exit plane exceeding 6% relative to the plain-wall baseline. This threshold ensures that the passive rib control does not penalize the propulsion system's thermodynamic efficiency while achieving base drag reduction.

Because the converged 5000-iteration base pressure predictions for Models A, B, and C now fall within a narrow band of one another (Section 4.4), the case for preferring the 3:1 configuration rests primarily on the total pressure loss criterion rather than on base-pressure magnitude alone. The thin 1 mm rib of Model A imposes the smallest physical blockage on the core stream of the three geometries; the SST k-ω contours (Appendix A) show the core flow maintaining a high-velocity, low-loss profile along the duct centreline, with the secondary rib vortices confined to the near-wall region and their wakes dissipating rapidly without extracting significant total pressure from the core. This is consistent with Rathakrishnan.,[1]finding that the 3:1 rib kept exit-plane total pressure losses within the 6% threshold.

For Models B and C, the taller ribs impose progressively greater blockage on the core stream, as evidenced by the more disrupted pressure fields in the Appendix B andAppendix C contours. Even though the converged base-pressure predictions for these geometries are now comparable to, and in the case of Model B, marginally deeper than those of Model A, the additional blockage from the 2 mm and 3 mm ribs is expected to extract a correspondingly larger total pressure penalty at the duct exit, plausibly approaching or exceeding the 6% threshold for Model C in particular. A precise numerical computation of exit-plane total pressure loss requires dedicated CFD post-processing of the area-weighted stagnation pressure field for each geometry, which remains recommended as a follow-on activity to definitively rank Models A, B, and C on an efficiency basis.

In summary, the updated, fully converged (5000-iteration) results confirm that all three rib geometries sustain sub-atmospheric base pressure at NPR = 2.458, with differences in base pressure magnitude among Models A, B, and C now within approximately 0.3% of one another. On this basis alone, the present 2D axisymmetric CFD study does not reproduce the pronounced 3:1 advantage and 3:2/3:3 degradation reported experimentally by Rathakrishnan.,[1]The 3:1 configuration (Model A) nonetheless remains the preferred candidate for aerospace base drag reduction applications on the grounds of minimal core-flow blockage and the associated expectation of the lowest total pressure loss, consistent with the 6% exit-plane efficiency criterion established in the literature.[2]

Conclusions

This study performed a 2D axisymmetric CFD verification of the experimental work by Rathakrishnan,[1] investigating the effect of internal annular ribs as a passive base-pressure control mechanism in a suddenly expanded duct with an area ratio of 6.25. Simulations were conducted in ANSYS Fluent across NPRs of 1.141 to 2.458, covering nozzle exit Mach numbers from 0.44 to 1.0, for three rib aspect ratio configurations: 3:1 (h = 1 mm), 3:2 (h = 2 mm), and 3:3 (h = 3 mm), with all final runs converged to 5000 iterations.

The SST k-ω turbulence model was selected following a preliminary sensitivity study (Section 4.1, Table 4.1 / Appendix D) in which all four candidate closures were evaluated at NPR = 2.458 across all three rib geometries. An initial assessment at 1000 iterations had produced physically unrealistic, strongly positive base pressures for the Standard k-ε and RNG k-ε models, and an apparent sign reversal for SST k-ω on the taller-rib geometries. Re-running all sixteen combinations to 5000 iterations resolved these issues: every closure now predicts a sub-atmospheric base pressure for every geometry, with values clustering between −31,450.3 Pa and −33,418.5 Pa. The SST k-ω model was retained as the primary closure because it consistently predicts the deepest base suction for every rib geometry (−33,330.03 Pa, −33,418.5 Pa, and −33,394.76 Pa for Models A, B, and C, respectively), converges earliest among the four closures, and is well supported by the literature for separated, adverse-pressure-gradient flows of this type.

The mesh independence study confirmed that a 0.5 mm structured quadrilateral mesh produces grid-independent results. The 2 mm mesh deviated by approximately 8.0% from the 0.5 mm reference at NPR = 11, exceeding the 5% independence threshold, while the 1 mm and 0.5 mm meshes agreed to within 0.78%. The 0.5 mm mesh was selected for all subsequent simulations.

The base pressure results, once converged to 5000 iterations, show all three rib configurations sustaining sub-atmospheric base pressure at NPR = 2.458 under SST k-ω: −33,330.03 Pa for Model A (3:1), −33,418.5 Pa for Model B (3:2), and −33,394.76 Pa for Model C (3:3). These values cluster within approximately 0.3% of one another, with Model B showing the marginally deepest suction, Model C close behind, and Model A the smallest of the three — though still the deepest prediction among all four turbulence models for its respective geometry. This represents a significant revision from the earlier 1000-iteration assessment, in which Models B and C appeared to reverse sign into pressurized, positive base regions accompanied by oscillatory or diverging residuals; the extended run length shows these earlier results to have been artifacts of insufficient convergence rather than genuine flow behavior.

The narrow-band convergence of base pressure across the 3:1 to 3:3 range only partially mirrors the experimental findings of Rathakrishnan,[1]whose study reported a pronounced 3:1 advantage and a marked degradation (sign reversal) for the 3:2 and 3:3 configurations, particularly at higher L/D ratios. The present steady, 2D axisymmetric RANS approach at a single NPR does not reproduce this degree of sensitivity, likely reflecting the limitations of a steady axisymmetric formulation in capturing the three-dimensional, transitionally unsteady mechanisms (such as horseshoe vortices around taller ribs) responsible for the experimental trend, as well as the fact that the experimental ranking incorporated wall-pressure oscillation and total pressure loss criteria in addition to base pressure magnitude.

Notwithstanding this narrower base-pressure spread, the 3:1 configuration (Model A) remains the recommended geometry for aerospace base drag reduction applications, on the basis that its thin 1 mm rib imposes the smallest blockage on the core stream and is therefore expected to incur the lowest total pressure loss at the duct exit plane, consistent with the 6% efficiency threshold established by Rathakrishnan.,[1] Quantitative computation of exit-plane total pressure loss for all three geometries is recommended as a priority follow-on activity to confirm this ranking and to fully reconcile the present converged base-pressure results with the experimental benchmark.

Acknowledgement

None.

Conflict of interest

Author has no conflicts of interest.

Funding

None.

References

1. Rathakrishnan E. Effect of ribs on suddenly expanded flows. *AIAA Journal*. 2001;39(7):1402–1404.
2. Khan A, Khan SA, Rajad V, et al. Effect of ribs in a suddenly expanded flow at sonic Mach number. *Heliyon*. 2024;10(11):e30313.